bioengineering

MDPI

Article

Effect of Pulse Frequency on the Microstructure and the Degradation of Pulse Electroformed Zinc for Fabricating the Shell of Biodegradable Dosing Pump

Shuhui Wu [1], Yizhuo Luo [1], Wei Hu [1], Yonghong Chen [2] and Zhi Huang [1,*]

[1] Institute of Biomedical Engineering, School of Basic Medical Sciences, Central South University, Changsha 410017, China; wushuhui@csu.edu.cn (S.W.); 8208191623@csu.edu.cn (Y.L.); 8208191624@csu.edu.cn (W.H.)
[2] Orthopedic and Traumatology Department, Chenzhou 3rd People's Hospital, Chenzhou 423000, China; gwstah@gmail.com
* Correspondence: biomaterials@csu.edu.cn

Abstract: In this work, we applied single-pulse electrodeposition method to prepare biodegradable zinc coating for the shell of an implantable dosing pump, and explored the effect of pulse frequency on microstructures and degradation behavior of electroformed zinc. Samples were produced by single-pulse electro-deposition technique with different pulse frequencies (50 Hz, 100 Hz, and 1000 Hz). By controlling the pulse frequency, the thickness of the zinc coating can be adjusted. The 50 Hz produced zinc film possesses strong (11.0) grain orientation, 100 Hz produced zinc film possesses clear ((11.0) and (10.0)) grain orientations, yet 1000 Hz produced zinc film shows more random grain orientations of (10.0), (10.1), and (11.0), which provides a possible way to design a controllable nanometer surface microtopography. Although thermodynamic degradation tendency implied from open current corrosion voltage were similar, the kinetic corrosion rate showed a clear increasing trend as pulse frequency increased from 50 Hz to 1000 Hz, which corresponded with the electrochemical impedance spectroscopy and long-term soaking test in hanks solution. According to ISO 10993-5:2009 and ISO 10993-4:2002, electrodeposited zinc materials produced in this study showed a benign hemolysis ratio and no toxicity for cell growth. Zinc prepared under 50 Hz shows the best blood compatibility. Electrodeposited zinc materials are expected to be used for the shell of a degradable dosing pump.

Keywords: zinc; coating; bioabsorbable; electroform

Citation: Wu, S.; Luo, Y.; Hu, W.; Chen, Y.; Huang, Z. Effect of Pulse Frequency on the Microstructure and the Degradation of Pulse Electroformed Zinc for Fabricating the Shell of Biodegradable Dosing Pump. *Bioengineering* **2022**, *9*, 289. https://doi.org/10.3390/bioengineering9070289

Academic Editor: Ali Zarrabi

Received: 13 May 2022
Accepted: 27 June 2022
Published: 29 June 2022

1. Introduction

Bioabsorbable metals and metal alloys are widely used in short-term implanted dosing pumps [1]. Zinc can be considered a candidate for the shell of implanted dosing pump because of its beneficial features [2]. Zinc is essential for normal basic functions of the body [3] and is also reported to be crucial to certain bio-functions such as immunity [4], osteogénesis [5], and keratinocyte migration [6]. In addition, zinc has specific and limited antibacterial properties [7]. Bowen has found that the degradation rate of pure zinc is suitable for clinical applications [8].

The continuous development of material processing technology and surface modification methods has promoted the research of medical devices with ideal mechanical, morphological and biocompatible [9] properties to meet functional requirements [10]. Appropriate coating of temporary biomedical implants could improve antibacterial properties [11], blood compatibility [12], osteogenesis, and tissue regeneration [13]. Materials commonly used to make coatings for biomedical implants include metals [14], polymers [15], and hydrogels [16]. Due to the low mechanical strength of pure zinc, it is not easy to fabricate a zinc layer with adjustable thickness with complex shape by conventional casting extrusion

methods. Electroplating zinc can be used as a coating on the surface of objects to play a protective role [17]. However, most of these galvanized coatings are less than 5 μm in thickness. Electro-deposition is a rapid proto-typing thin-wall coating technology, which can prepare coating with a thickness of 10 μm to 5 mm according to the thickness requirements [18]. The principle of electro-deposition is similar to electroplating, in which the anode is oxidized to provide cations, which are deposited on the cathode. The purpose of electroplating technology is to make coatings for decoration and reinforcement. In contrast, electro-deposition technology aims to produce an independent entity and the grain size of electro-deposition products is much smaller than that of casting products [19].

Some studies have used electrodeposition technology to produce composite electrodeposition zinc coating to optimize its performance [20], but most of them use direct current electrodeposition [21]. Surface morphology is a significant factor affecting the biocompatibility of implanted medical devices. Youssef, KMS et al. [22] studied the surface morphologies of pulse current electrodeposited nanocrystalline zinc, but they did not investigate the effect of pulse frequency on surface morphology. For one thing, energy and nucleation rate determine the preferred orientation during crystallization, for another pulsed current of different frequencies can provide different amounts of energy. The pulse frequency is likely to affect the surface morphology of the implanted devices. At present, there is no research on the application of electrodeposition technology in the preparation of implanted drug pump shells. In this study, we hypothesized that changing the pulse frequency would result in different surface morphology, degradation rate, and blood compatibility. Therefore, we hope to explore the effect of pulse frequency on microstructures and the degradation behavior of electroformed zinc and find a possible way to design a controllable nanometer surface microtopography for the shell of an implantable dosing pump suitable for clinical applications.

In this study, we used pulsed current electro-deposition to prepare a bioresorbable zinc coating layer for the shell of an implantable dosing pump with a thickness from 50 μm to 500 μm. Samples were produced by the single-pulse electrodeposition technique with different pulse frequencies (50 Hz, 100 Hz, 1000 Hz). The coatings were characterized by X-ray diffraction analyses (XRD), scanning electron microscope (SEM), polarization test, electrochemical impedance spectroscopy (EIS), and long-term static immersion test. Then the cytocompatibility and hemolytic rate of electroformed zinc was evaluated. We focused on the influence of pulse frequency on the microstructure, mechanical, and corrosion properties of electroformed zinc material and analyzed and discussed the experimental results.

2. Materials and Methods

2.1. Materials Preparation

The composition of the electro-deposition solution and operation conditions are shown in Table 1. The schematic diagram of the experiment device is shown in Figure 1. On electrodeposition, a commercially available zinc specimen (99% purity, 60 mm × 150 mm × 3 mm) was used as the anode. A 10 mm × 10 mm titanium plate was used as the cathode for forming zinc coating. Due to the low mechanical strength of zinc, we designed the zinc film with a thickness of 400 μm. The thickness of the zinc coating was controlled by modulating the time for electro-deposition. In this study, all samples were electrolytically deposited for 7 h. After electro-deposition under unidirectional pulsed current at different frequencies (50 Hz, 100 Hz, 1000 Hz), all as-prepared samples were immersed in 1% HNO_3 for about 2 s to remove the alkaline film on the surface of samples, then rinsed by deionized water and put into the natural-draft drier. Then the samples were carefully removed from the titanium electrode with a tweezer. The freshly prepared samples were used for SEM, XRD, polarization test, EIS, and long-term static immersion test.

Table 1. The composition of the electro-deposition solution and operation conditions.

Bath Composition	Range	Operation Conditions
$ZnSO_4 \cdot 7H_2O$	300–450 g/L	300 g/L γ = 30%
H_3BO_3	25–35 g/L	25 g/L t = 7 h
Brightening agent (S-Z95)	18–20 mg/L	19 mg/L
pH	3.5–5.5	4
Temperature	283–323 K	313 K
Cathode-current density	1–4 A/dm^2	4 A/dm^2
		Ton/Toff = 2/1

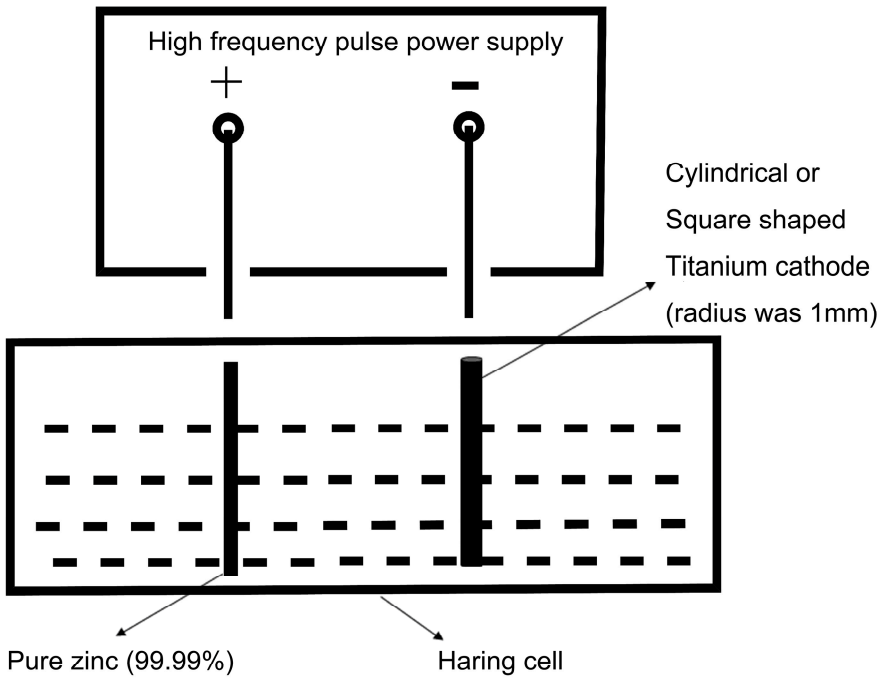

Figure 1. The schematic diagram of the experiment device.

2.2. Microstructure Characterization

The impact of different frequencies on grain orientation and morphology was analyzed using a scanning electron microscope (SEM, Quanta 250 FEG, FEI, USA) and X-ray diffraction analyses (XRD). XRD analyses were carried out using a Rigaku MiniFlex diffractometer, with Cu K_α radiation (1.54056 Å) to determine the grain size and the texture of the deposits. The scan rate was 0.02°/s over a 2θ ranging from 20° to 80°. The preferred orientation was calculated from the XRD spectrum. The preferred orientation of the obtained zinc samples was analyzed by Muresan's method [23]. If any crystal plane shows a T_c result bigger than 1, zinc will have the preferred orientation on this crystal plane.

The average grain size could be calculated by the Scherrer equation [24] (Equation (1)):

$$D = K\gamma / B\cos\theta \quad (1)$$

where D is the half-value breadth of the diffracted beam, K is a numerical constant that has the value of 0.93, γ is the X-Ray wavelength, B is the diffraction peak half-height width of the sample and θ is the Bragg angle.

2.3. Mechanical Test

The Vickers hardness of different pulse frequency electroformed zinc deposits (10 mm × 10 mm, mechanical polished) was conducted on Vickers micro hardness tester (HTV-PHS30, Foundrax, UK) at an applied load of 10 gf and indentation time of 15 s. As well, 6 measurements were taken at different positions on each zinc sample.

2.4. Static Immersion Test

The characterization of degradation behavior was measured by the immersion test. Four 5 mm × 5 mm zinc specimens were selected for each group prepared in different frequencies. Before the immersion test, all samples were ultrasonic cleaned in ethanol for 15 min and then in deionized water for 15 min. After drying the samples, weigh and record the weight of each sample. Then each zinc specimen was completely immersed in 50 mL of simulated body fluid Hank's solution [25] at 37 °C. After 30 days, 60 days, and 120 days of immersion, samples were precisely measured the weight loss. The immersion degradation rate of zinc specimens was calculated according to Equation (2):

$$V = (q_1 - q_0)/At\rho \quad (2)$$

where q_1 is the mass after immersion, q_0 is the mass before immersion, A is the surface area of the specimen, t is the immersion time, and ρ is the density of zinc.

2.5. Electrochemical Measurements

The polarization curves were tested using a three-electrode system (Ag/AgCl as reference electrode, 10 mm × 10 mm zinc plate as working electrode, Platinum as an auxiliary electrode with a surface area approximately two times as zinc plate) with CHI 600B electrochemical workstation. The theoretical degradation rate of zinc specimens was calculated by Faraday's Law [26]. The EIS test was then performed with the frequency ranging from 1 MHz to 10 KHz and analyzed its impedance data.

2.6. Cytocompatibility Evaluation

To investigate the feasibility of using electroformed zinc as the implantable materials, we accessed the cytocompatibility of electroformed zinc according to ISO10993-5:2009 [27]. Mesenchymal stem cells (MSC) and human umbilical vein endothelial cells (HUVEC) were chosen. For metal extract preparation, a metal plate with the geometric size of 10 mm × 10 mm was placed at the bottom of a 12-well flat-bottom plate, sterilized by UV light for 12 h. Then extracts were cultured for 24 h at 37 °C. Then we added 200 μL as-prepared metal supernatant into each well and cultured it with 1×10^4 cells for 3 days. Finally, an MTT kit was used to detect cell activity. Three samples were taken from each group of different frequencies (50 Hz, 100 Hz, 1000 Hz) for cytocompatibility tests.

2.7. Hemolysis Evaluation

Diluted blood for hemolysis evaluation was prepared with healthy adult blood from a male volunteer. All the experiments were approved by the medical ethics committee of Xiangya III Hospital of Central South University (No. 2016-S139). Pure zinc samples were smashed and dipped in a 10 mL 0.9% NaCl solution for 30 min. A 0.9% NaCl solution was prepared as the negative control. Deionized water was prepared as the positive control. After incubation with 0.2 mL blood, zinc metals were removed, and the supernatant in each tube was measured by ultraviolet spectrophotometer at 545 nm. Three samples were taken from each group of different frequencies (50 Hz, 100 Hz, 1000 Hz) for hemolysis evaluation. The hemolysis result could be calculated using the formula as follows [28]:

$$\text{Hemolysis} = (\text{OD}_{\text{test}} - \text{OD}_{\text{neg}})/(\text{OD}_{\text{pos}} - \text{OD}_{\text{neg}}) \quad (3)$$

where OD was the optical density at 545 nm.

2.8. Statistic Analysis

Data are presented as a mean ± standard deviation and a one-way analysis of variance (ANOVA) was employed with a Tukey's HSD posthoc test using Graphpad version 7.4 software. A value of $p < 0.05$ was considered significant.

3. Results and Discussion

Figure 2 shows the theoretical and actual thicknesses in experiments of the electrodeposited sample. The *p* values between the calculated groups were all less than 0.05, indicating that the data differences between the groups were significant. With the increase of pulse frequency from 50 Hz to 1000 Hz, the thickness of the electrodeposited zinc layer decreased from 396 µm to 363 µm. Higher pulse frequency leads to a lower energy conversion rate, and therefore lower zinc formation efficiency. Such phenomenon is due to the zinc deposition kinetic processes during pulse electro-deposition. The primary technique adopted in this experiment is single-pulse electro-deposition. During one pulse cycle, charging time and pulse duration time inverse the pulse frequency. The double electric layer is formed during charging and acts as a resistance at the beginning of each pulse. According to the capacitance effect theory mentioned by Gülesin Yılmaz [29], the charging time and discharging time are much shorter than the whole pulse duration, and owing to the increasing pulse frequency, the considerable accumulation of capacitive effect reduces the energy efficiency. Therefore, the energy efficiency decreases correspondingly as pulse frequency increase, thus making the thickness of electro-deposition zinc decrease with the increase of pulse frequency.

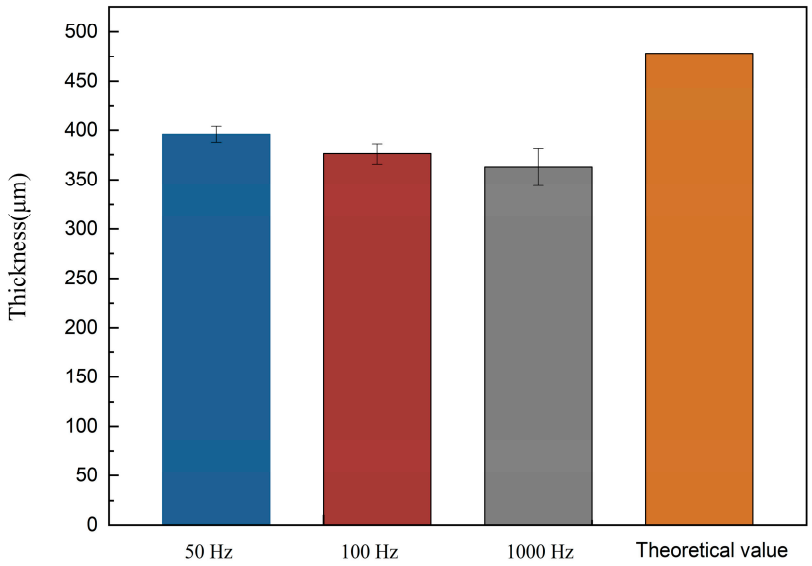

Figure 2. The theoretical and real thickness of electroformed zinc.

The XRD patterns identified the samples electrolytically deposited under 50 Hz, 100 Hz, and 1000 Hz pulse frequency as pure zinc (PDF NO.04-0831) with a hexagonal close-packed (hcp) crystal structure in Figure 3. The average grain size of the coating is estimated by the Scherrer equation, which is 641 Å in 50 Hz, 457 Å in 100 Hz, and 387 Å in 1000 Hz. Moreover, all the samples exhibited considerably high crystallinity with the remarkably high sharpness of the XRD patterns.

To explore the preferred orientation of the electrodeposited zinc deposit, the texture coefficient was calculated according to Muresan's method [30]. The corresponding texture coefficient (Tc) values are shown as a bar chart in Figure 4. According to Muresan's method, the Tc value above 1 refers to the preferred orientation of a certain plane. Figure 4 shows that (11.0) and (10.0) are the preferred orientation for all frequencies.

The atom density of the (11.0) plane is relatively higher than that of the (10.0) or (10.1) plane in hcp structure, and the surface energy of the (10.0) or (10.1) plane is lower than that of the (11.0) plane [31]. The Tc value of (11.0) at 50 Hz is much higher than 100 Hz and 1000 Hz. When frequency arises from 50 Hz to 1000 Hz, the Tc value of (10.1) and (10.2) increases, while the Tc value of (11.0) and (10.3) decreases. During crystallization, energy and nucleation rate determine the preferred orientation. In the normal crystallization

process, where energy dominate, atoms always tend to crystallize in the (00.2) plane due to the lowest surface energy. However, the electroplating process provides sufficient energy, and the nucleation rate becomes more important. If the increased fresh metal atoms do not migrate to the (10.0) plane, then some of these atoms could stay at the (11.0) plane thus the orientation is changed. As mentioned above, a lower frequency means a relatively longer T_{off} and T_{on}, and according to the capacitive effect, more energy is charged to the samples under 50 Hz. Then a more rapid nucleation rate exists under 50 Hz. Finally, the (11.0) plane becomes dominant for the samples electrolytically deposited under 50 Hz. But such an effect is less obvious for the 1000 Hz sample as less energy is inputted to the system, which makes zinc film exhibit more random orientations at 1000 Hz [32] and the Tc value of the (11.0) plane decreased. This finding could be further studied to control desirable surface conditions for the implantable electronic device material.

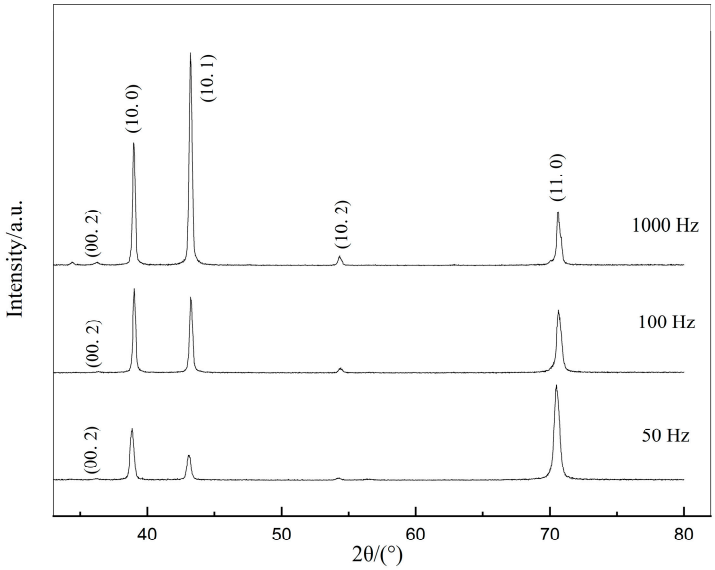

Figure 3. XRD patterns of electrodeposited zinc under 50 Hz, 100 Hz, and 1000 Hz pulse frequency.

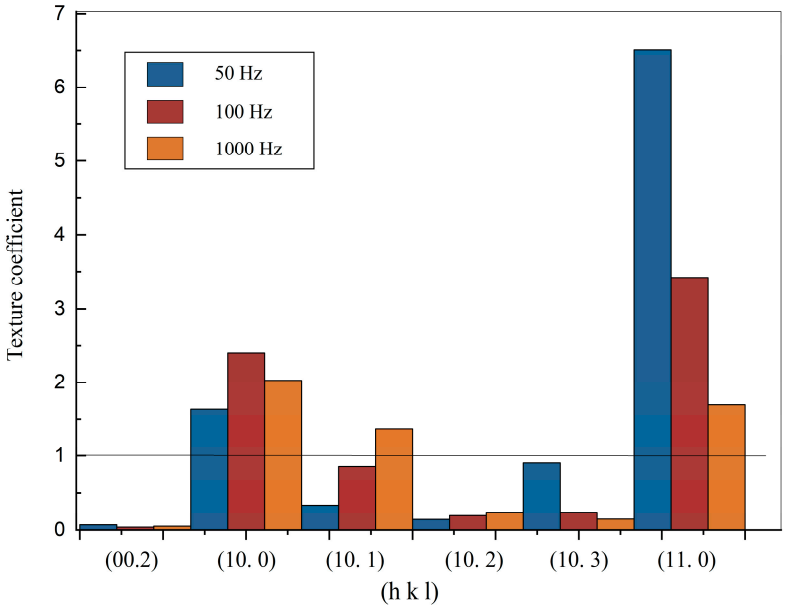

Figure 4. Tc chart of electrodeposited zinc under 50 Hz, 100 Hz, 1000 Hz pulse frequency.

Figure 5 shows the SEM images of the surface morphology of zinc films which are electrolytically deposited under 50 Hz, 100 Hz, and 1000 Hz pulse frequency. The electrodeposited zinc materials all showed metallic brightness and smooth surface observed with naked eyes, but when magnified by SEM, the samples exhibited an anisotropic dendritic morphology. Figure 5 represents grain obtained under 1000 Hz pulse frequency tends to grow more randomly compared to zinc film under 50 Hz and 100 Hz, which is consistent with the Tc results in Figure 4. Both XRD and SEM results indicate that frequency has effects on the grain orientations for electrodeposited zinc, and in our case, reducing PC frequency would help to grow the preferred orientation in zinc, and versa.

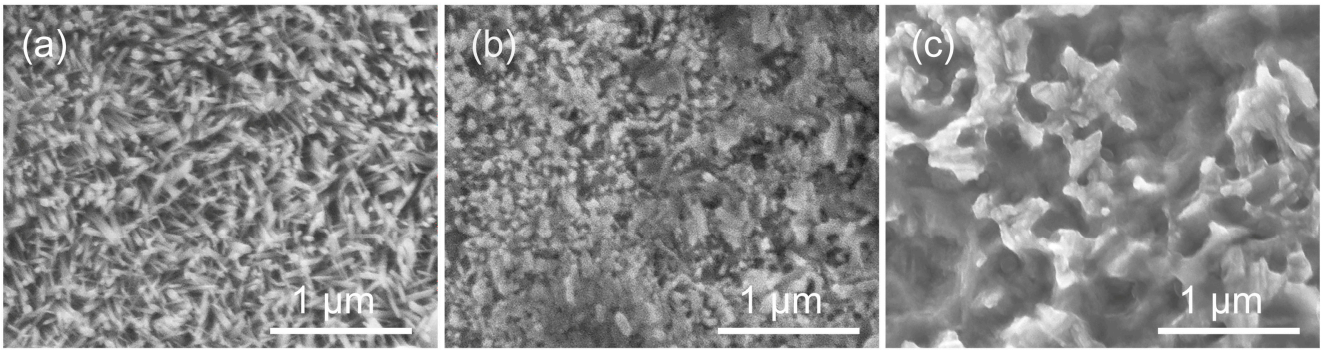

Figure 5. SEM of electrodeposited zinc film: (**a**–**c**) are under 50 Hz, 100 Hz, and 1000 Hz, respectively.

Figure 6 shows the SEM images of the cross-section of deposited coatings under 100 Hz and 1000 Hz. The grain orientation can not be seen from the cross-section image, but it can be seen that the matrix formed by electrodeposition is very dense, which can effectively prevent the infiltration of water and water vapor.

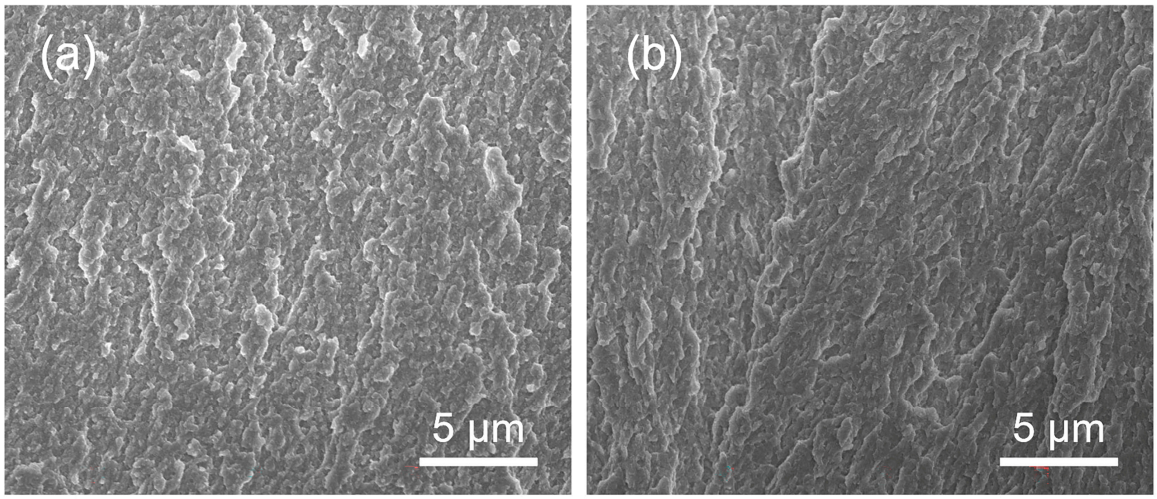

Figure 6. SEM of the cross-section of deposited coating: (**a**,**b**) are under 100 Hz and 1000 Hz, respectively.

Higher hardness of coating for implantable electronic devices is desirable, as it secures the electrodeposited layer structural functionality. Figure 7 shows the bar chart of Vickers hardness of pure electrodeposited zinc under different PC frequencies. The microhardness of the three samples is almost the same. In addition, electrodeposited zinc shows better performance (~48 HV) than normal zinc (37 HV) [33].

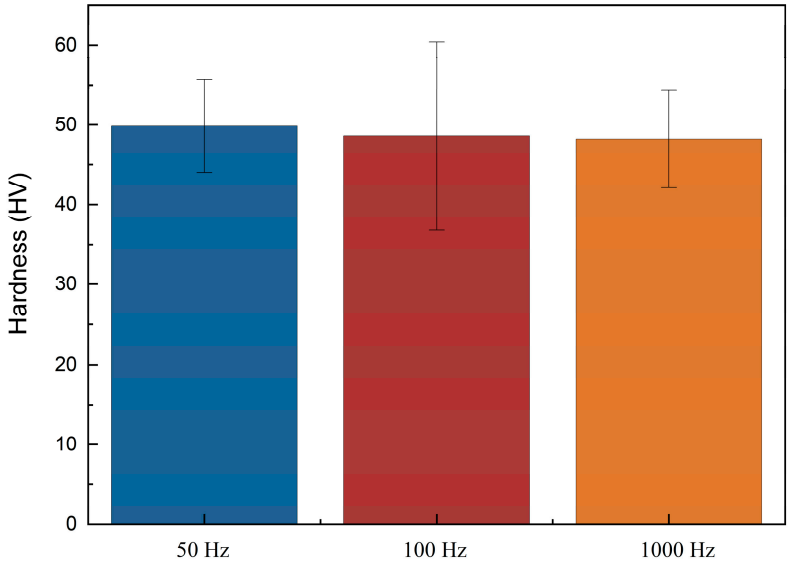

Figure 7. Bar chart of Vickers hardness of electrodeposited zinc under 50 Hz, 100 Hz, and 1000 Hz.

The corrosion properties could be detected by Tafel curves, where the E_{corr} and I_{corr} are the most important parameters which can serve as theoretical predictions. Figure 8 shows the Tafel plot test of three samples carried out in CHI660B electrochemical station. It can be seen from Table 2, the calculated Tafel slope reveals that zinc under 50 Hz shows a slightly lower Tafel slope than zinc under 100 Hz and 1000 Hz, which indicates the lower corrosion rate of 50 Hz zinc due to the higher activation energy, though the difference is not significant. Table 2 lists the annual corrosion rate calculated by Faraday's law. E_{corr} of zinc under 50 Hz, 100 Hz, and 1000 Hz are close, which indicates the similar corrosion tendency of zinc prepared under different PC frequencies. As the pulse frequency changes from 50 Hz to 1000 Hz, the annual corrosion rate gradually increases from 0.11182 mm/year·cm^2 to 0.12779 mm/year·cm^2, which shows a non-significant increasing trend and is similar to as-cast pure Zinc (0.132 mm/year·cm^2) [26].

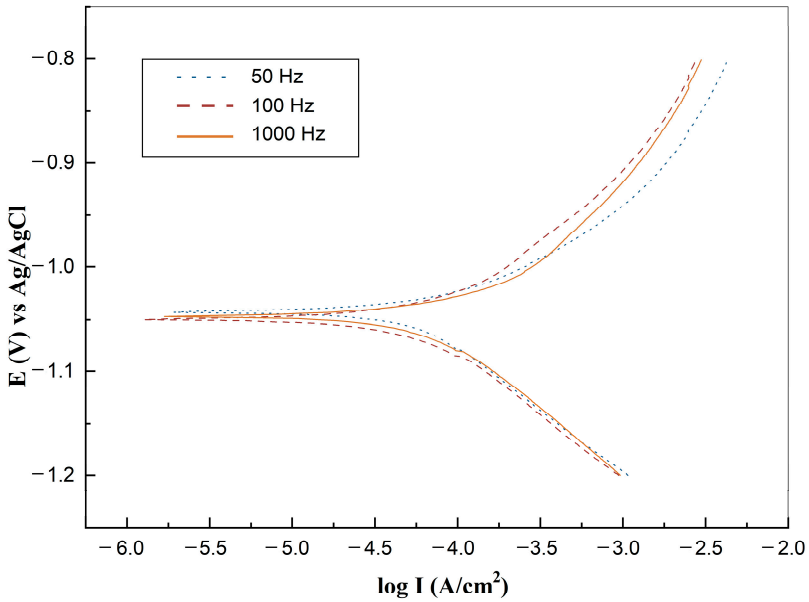

Figure 8. Tafel plot of zinc under 50 Hz, 100 Hz, and 1000 Hz, respectively (37 °C immersed in Hank's solution for 30 min).

Table 2. Electrochemical parameters of zinc under 50 Hz, 100 Hz, and 1000 Hz, respectively.

Samples (Hz)	βa (mV/decade)	βb (mV/decade)	Icorr (10^{-6} A/cm^2)	Ecorr (V)	C (mm·year^{-1}·cm^2)
50	15.148	8.118	7.993	−1.0427	0.11182
100	16.155	8.334	8.134	−1.0497	0.12092
1000	16.388	8.445	8.596	−1.0474	0.12779

After the electrochemical test, a long-term simulation degradation test should be conducted to testify to the degradation property of certain materials. We conducted immersion tests for up to 120 d in Hank's solution. As indicated in Figure 9, the degradation rate of zinc samples electrolytically deposited under a pulse frequency of 1000 Hz is higher than zinc samples electrolytically deposited under 100 Hz and 50 Hz. A positive correlation between degradation rates and immersion time is found. All electrodeposited zinc samples show accelerated degradation behavior. Interestingly, this phenomenon is more apparent when the immersion time changes from 30 days to 60 days, which means the degradation rate accelerated with prolonged soaking time, despite the corrosion product layer formed during corrosion. However, only the 30-day degradation rates are lower than bulk zinc (0.0438 mm year^{-1}) [34], and the 60-day and 120-day degradation rates are similar to the literature values.

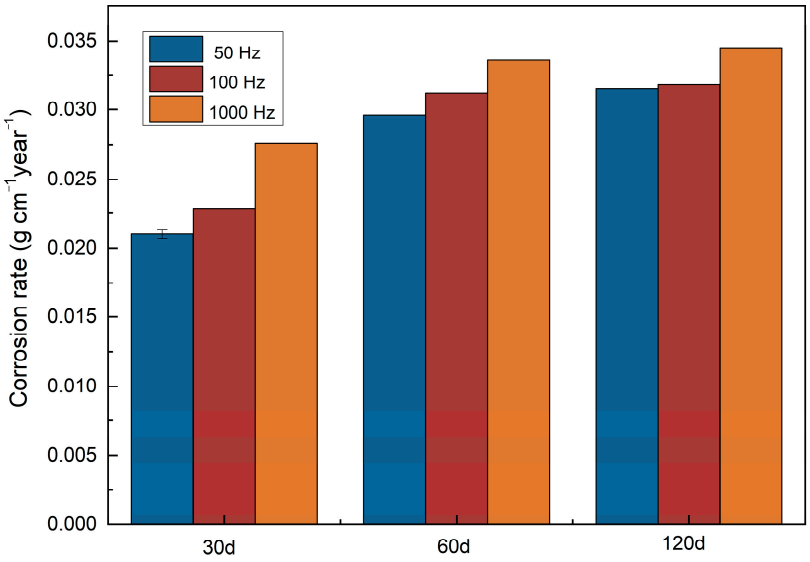

Figure 9. Degradation rates of electrodeposited zinc for 30, 60, and 120 days.

To further address the difference in degradation rate, as shown in Figures 8 and 9, EIS measurements in Hank's solution (37 °C) were conducted. The impedance diagram is shown as a Nyquist plot in Figure 10. The equivalent circuit fitted to study impedance spectra is shown in Figure 11. Mou Cheng Li et al. [35] obtained a similar equivalent circuit of zinc in 3.5% NaCl solutions. Table 3 indicates the impedance parameters.

The zinc sample electrolytically deposited under 50 Hz pulse possesses higher Rp and lower double-layer capacitance than zinc samples under 100 Hz and 1000 Hz, the Rp value increases in the order 1000 Hz < 100 Hz < 50 Hz. Thus, the order of samples corrosion resistance is 50 Hz < 100 Hz < 1000 Hz, which is coincidental with Tafel plots. The impedance data from Table 3 indicates the significant improvement of polarization resistance on 1000 Hz zinc samples after the static immersion test. EDAX results show the increased concentration of O and the existence of elements C and Zn on the 1000 Hz static immersed zinc sample. From SEM characterization and L Yin's work [34], we understood that upon being immersed in Hank's solution, zinc quickly reacts with the

acid components, forming a porous layer consisting of ZnO, $Zn(OH)_2$, and other chloride corrosion products [35].

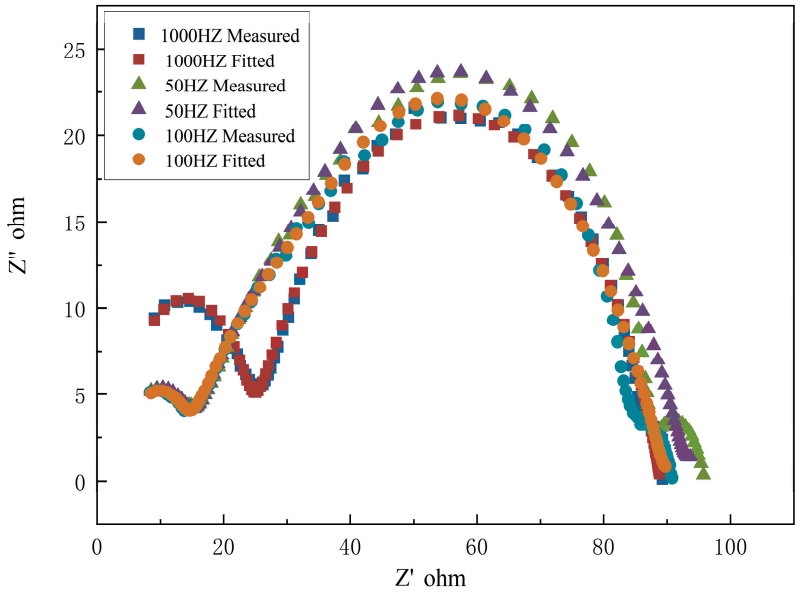

Figure 10. Nyquist plot of zinc under 50 Hz, 100 Hz, and 1000 Hz.

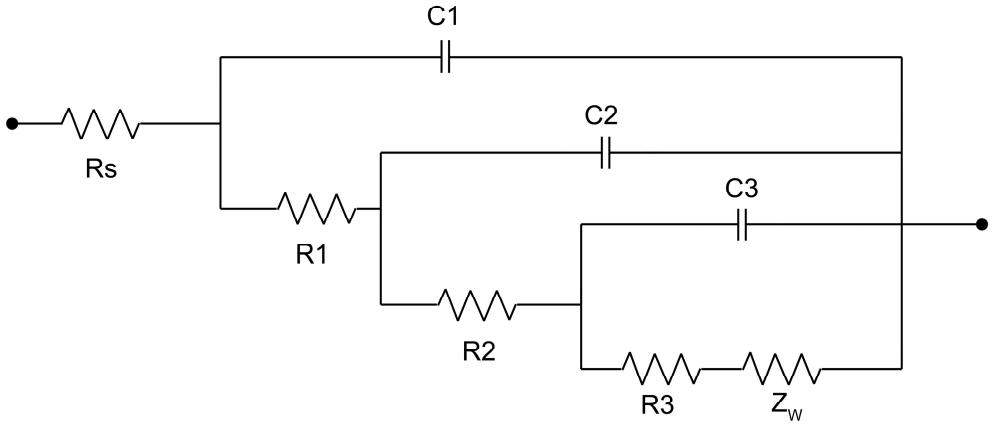

Figure 11. The equivalent circuit used to fit the Nyquist plot in Figure 9.

Table 3. Impedance parameters.

F (Hz)	Rs ($\Omega \cdot cm^2$)	C1 ($\mu F \cdot cm^{-2}$)	R1 ($\Omega \cdot cm^2$)	C2 ($\mu F \cdot cm^{-2}$)	R2 ($\Omega \cdot cm^2$)	C3 ($\mu F \cdot cm^{-2}$)	R3 ($\Omega \cdot cm^2$)	Rp * ($\Omega \cdot cm^2$)
50	4.664	0.1916	10.22	184.1	49.65	41.89	28.45	88.32
100	4.425	0.1849	9.857	21.84	48.21	57.28	27.12	85.19
1000	4.582	0.1301	8.82	135.7	47.57	82.59	27.8	83.65

* Polarization resistance (RP) is the sum of all three resistances R1, R2, and R3.

The surface morphologies of both original and soaked zinc films (1000 Hz) in Figure 12 clearly illustrate the effect of corrosion on surface conditions. Figure 12a shows some pseudo-hexagonal plane crystals on the zinc coating samples. The white porous corrosion product layer on the metal substrate during immersion is observed in Figure 12b. After the immersion test, the crystals grow and form islands that spread over the entire surface.

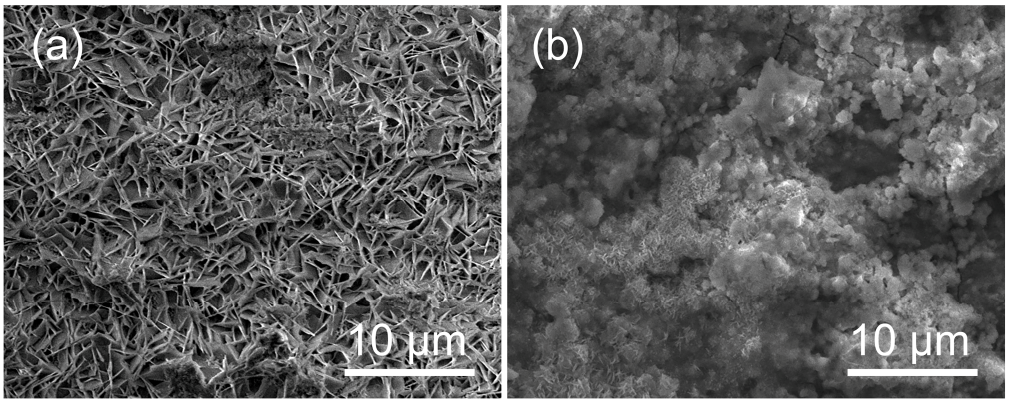

Figure 12. SEM of zinc film after electrochemical impedance studies: (**a**) 1000 Hz zinc before static immersion test. (**b**) 1000 Hz zinc after 30 day's static immersion test.

The difference in degradation rate could be explained by the electro-deposition process of zinc. Girin [31] and Jantaping [36] reported that zinc coatings with a prismatic (11.0) texture have better corrosion resistance than other coatings. According to their study, the zinc layer with (11.0) texture promotes the formation of the amorphous-oxide layer, and this formed amorphous-oxide layer plays an effective protective barrier role which could effectively reduce the corrosion of zinc samples. In the corrosive environment, the corrosion rate of each zinc metal grain varies because of the difference in the binding energy of atoms between the crystallographic planes [37]. Mouanga successfully inhibited the corrosion of zinc by using urea; the presence of urea leads to the increase of (11.2) plane's intensity [38]. In our study, zinc film prepared under 50 Hz pulse frequency showed obviously (11.0) preferred orientation, which may be the reason for the better anti-corrosion performance of 50 Hz-zinc than the others.

As shown in Figure 13, in the cytocompatibility evaluation, the toxic effects on the cell viability of MSC are higher than those on HUVEC. The toxic effects on the cell viability of all the electrodeposited zinc samples do not significantly differ. S-295 brightener was used in the preparation process of electrolytic deposition, and there was inevitable residue. However, the cytocompatibility evaluation results indicate that electrodeposited zinc materials do not present any toxic effects on MSC and HUVEC cells and exhibit excellent biocompatibility, which is in good consistent with the results of coating fabricated by the conventional casting methods [39].

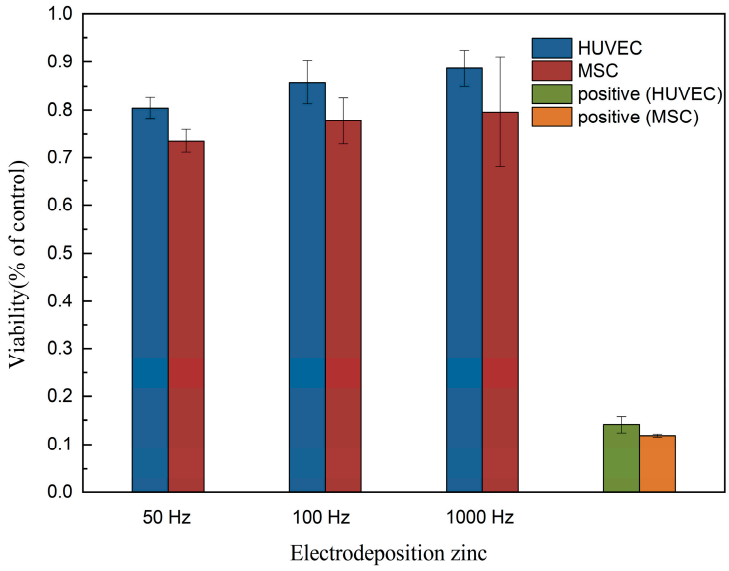

Figure 13. The cytotoxicity of electrodeposited zinc.

Table 4 shows the results of the hemolysis test. The calculated hemolysis rates of zinc (50 Hz, 100 Hz, and 1000 Hz) are 0.478%, 1.368%, and 0.752%, respectively, which are far less than the safe value of 5%, suggesting that the electrodeposited zinc materials would not lead to severe hemolysis according to ISO 10993-4:2002. Among them, zinc prepared under 50 Hz shows the best blood compatibility. One possible explanation is that the microphase structure with certain roughness can sometimes obtain extremely high blood compatibility, and the material with heterogeneous microphase structure in the range of 0.1~2 μm has better anticoagulant properties [40]. According to Figure 5, the surface grain size of zinc under 50 Hz is 0.628 ± 0.095 μm, and the surface grains show an anisotropic arrangement and heterogeneous microfacies structure.

Table 4. The hemolysis test of electrodeposited zinc.

	50 Hz	100 Hz	1000 Hz	Positive Control	Blank Control
OD (A)	0.043	0.056	0.047	0.036	1.498
T (%)	90.7	87.7	89.7	91.8	3.1
Hemolysis rate	0.478	1.368	0.752	-	-

OD: optical density; T: transmittance.

4. Conclusions

In this study, the way to control the thickness of zinc films by electro-deposition time management has been found and used to produce 50 μm~500 μm zinc films, successfully. Pulse electrodeposited zinc materials with different preferred grain orientations and microstructures were produced by varying pulse frequencies to 50 Hz, 100 Hz, and 1000 Hz. The main conclusions are as follows.

1. The thickness can be adjusted by electrodeposition, which is convenient and controllable, and the product has no cracking phenomenon.
2. The test results also imply that pulse frequency will affect the grain orientation, and thus the corrosion properties. It is shown that the 50 Hz produced zinc film possesses strong (11.0) grain orientation, 100 Hz produced zinc film possesses clear (11.0) and (10.0) grain orientations, yet 1000 Hz produced zinc film shows more random grain orientations of (10.0), (10.1) and (11.0).
3. The effect of the pulse frequency resulting from microstructures was clarified by electrochemical tests. Although thermodynamic degradation tendency implied from open current corrosion voltage (E_{corr}) were similar, the kinetic corrosion rate showed a clear increasing trend as pulse frequency increased from 50 Hz to 1000 Hz, which corresponded with the EIS test and long-term soaking test in hanks solution. This tendency is probably attributed to the refined grain that increased the structural stability of the PC-formed zinc. It provides a possible way to design a controllable nanometer surface microtopography by adjusting PC frequency.
4. Our results also indicated that appropriate pulse frequency can improve the blood compatibility of the material. According to ISO 10,993-5:2009 and ISO 10993-4:2002, electrodeposited zinc materials produced in this study showed a benign hemolysis ratio and no toxicity for cell growth. Zinc prepared under 50 Hz shows the best blood compatibility. Electrodeposited zinc materials are expected to be used for the shell of a degradable dosing pump.

Author Contributions: Conceptualization, S.W. and Y.L.; methodology, S.W.; software, S.W. and Y.L.; validation, S.W. and Y.L.; formal analysis, S.W.; investigation, S.W. and Y.L.; resources, Z.H.; data curation, W.H.; writing—original draft preparation, S.W.; writing—review and editing, S.W.; visualization, S.W.; supervision, Z.H.; funding acquisition, Y.C. All authors have read and agreed to the published version of the manuscript.

Funding: This research was funded by National Natural Science Foundation of China, (No. 81641085, 81301536); Hunan Provincial Natural Science Foundation of China (No. 11JJ1008); Science and Technology Development Plan Project of Chenzhou (No. zdyf201993).

Institutional Review Board Statement: Not applicable.

Informed Consent Statement: Not applicable.

Data Availability Statement: The data that support the findings of this study are available from the corresponding author upon reasonable request. All figures in this paper are original.

Conflicts of Interest: The authors declare no conflict of interest.

References

1. Ryu, H.; Seo, M.H.; Rogers, J.A. Bioresorbable Metals for Biomedical Applications: From Mechanical Components to Electronic Devices. *Adv. Healthc Mater.* **2021**, *10*, e2002236. [CrossRef] [PubMed]
2. Liu, L.; Meng, Y.; Dong, C.; Yan, Y.; Volinsky, A.A.; Wang, L.-N. Initial formation of corrosion products on pure zinc in simulated body fluid. *J. Mater. Sci. Technol.* **2018**, *34*, 2271–2282. [CrossRef]
3. Sawidis, T.; Yurukova, L.; Askitis, T. Chios mastic, a natural supplement for zinc to enhance male sexuality and prostate function. *Pharm. Biol.* **2010**, *48*, 48–54. [CrossRef] [PubMed]
4. Dardenne, M. Zinc and immune function. *Eur. J. Clin. Nutr.* **2002**, *56*, S20–S23. [CrossRef] [PubMed]
5. Moonga, B.S.; Dempster, D.W. Zinc is a potent inhibitor of osteoclastic bone resorption in vitro. *J. Bone Miner. Res.* **1995**, *10*, 453–457. [CrossRef]
6. Tenaud, I.; Saiagh, I.; Dreno, B. Addition of zinc and manganese to a biological dressing. *J. Dermatol. Treat.* **2009**, *20*, 90–93. [CrossRef]
7. Su, Y.C.; Wang, K.; Gao, J.L.; Yang, Y.; Qin, Y.X.; Zheng, Y.F.; Zhu, D.H. Enhanced cytocompatibility and antibacterial property of zinc phosphate coating on biodegradable zinc materials. *Acta Biomater.* **2019**, *98*, 174–185. [CrossRef]
8. Bowen, P.K.; Drelich, J.; Goldman, J. Zinc exhibits ideal physiological corrosion behavior for bioabsorbable stents. *Adv. Mater.* **2013**, *25*, 2577–2582. [CrossRef]
9. Zhou, Y.; Wang, J.W.; Yang, Y.W.; Yang, M.L.; Zheng, H.Z.; Xie, D.Q.; Wang, D.S.; Shen, L.D. Laser Additive Manufacturing of Zinc Targeting for Biomedical Application. *Int. J. Bioprinting* **2022**, *8*, 501. [CrossRef]
10. Betancourt, T.; Brannon-Peppas, L. Micro- and nanofabrication methods in nanotechnological medical and pharmaceutical devices. *Int. J. Nanomed.* **2006**, *1*, 483–495. [CrossRef]
11. Yuan, Z.; He, Y.; Lin, C.; Liu, P.; Cai, K. Antibacterial surface design of biomedical titanium materials for orthopedic applications. *J. Mater. Sci. Technol.* **2021**, *78*, 51–67. [CrossRef]
12. Badv, M.; Bayat, F.; Weitz, J.I.; Didar, T.F. Single and multi-functional coating strategies for enhancing the biocompatibility and tissue integration of blood-contacting medical implants. *Biomaterials* **2020**, *258*, 25. [CrossRef] [PubMed]
13. del Olmo, J.A.; Perez-Alvarez, L.; Pacha-Olivenza, M.A.; Ruiz-Rubio, L.; Gartziandia, O.; Vilas-Vilela, J.L.; Alonso, J.M. Antibacterial catechol-based hyaluronic acid, chitosan and poly (*N*-vinyl pyrrolidone) coatings onto Ti6Al4V surfaces for application as biomedical implant. *Int. J. Biol. Macromol.* **2021**, *183*, 1222–1235. [CrossRef] [PubMed]
14. Moravej, M.; Mantovani, D. Biodegradable metals for cardiovascular stent application: Interests and new opportunities. *Int. J. Mol. Sci.* **2011**, *12*, 4250–4270. [CrossRef]
15. Flejszar, M.; Chmielarz, P. Surface Modifications of Poly(Ether Ether Ketone) via Polymerization Methods—Current Status and Future Prospects. *Materials* **2020**, *13*, 999. [CrossRef]
16. Fu, M.; Liang, Y.; Lv, X.; Li, C.; Yang, Y.Y.; Yuan, P.; Ding, X. Recent advances in hydrogel-based anti-infective coatings. *J. Mater. Sci. Technol.* **2021**, *85*, 169–183. [CrossRef]
17. Song, Y.; Tang, J.; Hu, J.; Yang, H.; Gu, W.; Fu, Y.; Ji, X. Interfacial assistant role of amine additives on zinc electrodeposition from deep eutectic solvents: An in situ X-ray imaging investigation. *Electrochim. Acta* **2017**, *240*, 90–97. [CrossRef]
18. Moravej, M.; Prima, F.; Fiset, M.; Mantovani, D. Electroformed iron as new biomaterial for degradable stents: Development process and structure–properties relationship. *Acta Biomater.* **2010**, *6*, 1726–1735. [CrossRef]
19. Wu, G.; Li, N.; Zhou, D.; Mitsuo, K. Mitsuo Microstructure of Co-Ni-Al_2O_3 Composite Coatings by Electroforming. *J. Mater. Sci. Technol.* **2003**, *19*, 133–134.
20. Kumar, C.M.P.; Lakshmikanthan, A.; Chandrashekarappa, M.P.G.; Pimenov, D.Y.; Giasin, K. Electrodeposition Based Preparation of Zn-Ni Alloy and Zn-Ni-WC Nano-Composite Coatings for Corrosion-Resistant Applications. *Coatings* **2021**, *11*, 17. [CrossRef]
21. Kumar, C.M.P.; Chandrashekarappa, M.P.G.; Kulkarni, R.M.; Pimenov, D.Y.; Giasin, K. The Effect of Zn and Zn-WO3 Composites Nano-Coatings Deposition on Hardness and Corrosion Resistance in Steel Substrate. *Materials* **2021**, *14*, 2253. [CrossRef] [PubMed]
22. Youssef, K.M.S.; Koch, C.C.; Fedkiw, P.S. Improved corrosion behavior of nanocrystalline zinc produced by pulse-current electrodeposition. *Corros. Sci.* **2004**, *46*, 51–64. [CrossRef]
23. Muresan, L.; Oniciu, L.; Froment, M.; Maurin, G. Inhibition of lead electrocrystallization by organic additives. *Electrochim. Acta* **1992**, *37*, 2249–2254. [CrossRef]
24. Patterson, A.L. The Scherrer Formula for X-ray Particle Size Determination. *Phys. Rev.* **1939**, *56*, 978–982. [CrossRef]

25. Hanks, J.H.; Wallace, R.E. Relation of Oxygen and Temperature in the Preservation of Tissues by Refrigeration. *Proc. Soc. Exp. Biol. Med.* **1949**, *71*, 196–200. [CrossRef]
26. Li, H.F.; Xie, X.H.; Zheng, Y.F.; Cong, Y.; Zhou, F.Y.; Qiu, K.J.; Wang, X.; Chen, S.H.; Huang, L.; Tian, L.; et al. Development of biodegradable Zn-1X binary alloys with nutrient alloying elements Mg, Ca and Sr. *Sci. Rep.* **2015**, *5*, 10719. [CrossRef]
27. Liu, X.; Sun, J.; Yang, Y.; Pu, Z.; Zheng, Y. In vitro investigation of ultra-pure Zn and its mini-tube as potential bioabsorbable stent material. *Mater. Lett.* **2015**, *161*, 53–56. [CrossRef]
28. Li, B.; Chen, Y.; Huang, W.; Yang, W.Z.; Yin, X.S.; Liu, Y. In vitro degradation, cytocompatibility and hemolysis tests of CaF_2 doped TiO_2-SiO_2 composite coating on AZ31 alloy. *Appl. Surf. Sci.* **2016**, *382*, 268–279. [CrossRef]
29. Yılmaz, G.; Hapçı, G.; Orhan, G. Properties of Ni/Nano-TiO_2 Composite Coatings Prepared by Direct and Pulse Current Electroplating. *J. Mater. Eng. Perform.* **2015**, *24*, 709–720. [CrossRef]
30. Fustes, J.; Gomes, A.; Pereira, M.I.D. Electrodeposition of Zn-TiO_2 nanocomposite films-effect of bath composition. *J. Solid State Electrochem.* **2008**, *12*, 1435–1443. [CrossRef]
31. Girin, O.; Panasenko, S. Influence of the texture of electrolytic zinc coatings on their corrosion resistance. *Prot. Met.* **1989**, *25*, 480–482.
32. Chen, L.; Wang, L.; Zeng, Z.; Xu, T. Influence of pulse frequency on the microstructure and wear resistance of electrodeposited Ni-Al_2O_3 composite coatings. *Surf. Coat. Technol.* **2006**, *201*, 599–605. [CrossRef]
33. Kurdowski, W.; Bochenek, A. Three principles of concrete corrosion prevention. *Cem. Wapno Beton* **2012**, *17*, 434–442.
34. Yin, L.; Cheng, H.; Mao, S.; Haasch, R.; Liu, Y.; Xie, X.; Hwang, S.W.; Jain, H.; Kang, S.K.; Su, Y. Dissolvable metals for transient electronics. *Adv. Funct. Mater.* **2014**, *24*, 645–658. [CrossRef]
35. Li, M.C.; Jiang, L.L.; Zhang, W.Q.; Qian, Y.H.; Luo, S.Z.; Shen, J.N. Electrochemical corrosion behavior of nanocrystalline zinc coatings in 3.5% NaCl solutions. *J. Solid State Electrochem.* **2007**, *11*, 1319–1325. [CrossRef]
36. Jantaping, N.; Schuh, C.A.; Boonyongmaneerat, Y. Influences of crystallographic texture and nanostructural features on corrosion properties of electrogalvanized and chromate conversion coatings. *Surf. Coat. Technol.* **2017**, *329*, 120–130. [CrossRef]
37. Park, H.; Szpunar, J.A. The role of texture and morphology in optimizing the corrosion resistance of zinc-based electrogalvanized coatings. *Corros. Sci.* **1998**, *40*, 525–545. [CrossRef]
38. Mouanga, M.; Ricq, L.; Douglade, J.; Berçot, P. Effects of some additives on the corrosion behaviour and preferred orientations of zinc obtained by continuous current deposition. *J. Appl. Electrochem.* **2007**, *37*, 283–289. [CrossRef]
39. Otani, T.; Nagata, M.; Fukunaka, Y.; Homma, T. Morphological evolution of mossy structures during the electrodeposition of zinc from an alkaline zincate solution. *Electrochim. Acta* **2016**, *206*, 366–373. [CrossRef]
40. Zhang, A.X.; Lv, D.L.; Zhong, W.; Cheng, W.Z.; Du, Q.G. Blood Compatibility of Biomaterials. *Prog. Biomed. Eng.* **2004**, *25*, 53–58.